https://doi.org/10.5194/egusphere-2025-5357
Preprint. Discussion started: 23 January 2026

G&M3D 1.0: an Interactive Framework for 3D Model Construction and Forward Calculation of Potential Fields

Dengkang Wang[1], Bo Chen[1,2,3], Kanggui Wei[4], Jiaxiang Peng[1] and Rongwen Guo[1,2,3]

[1]School of Geosciences and Info-Physics, Central South University, Changsha 410083, China
[2]Hunan Key Laboratory of Non-ferrous Resources and Geological Hazard Detection, Changsha 410083, China
[3]Key Laboratory of Metallogenic Prediction of Nonferrous Metals and Geological Environment Monitoring (Central South University), Ministry of Education, Changsha 410083, China
[4]Engineering Laboratory for Deep Resources Equipment and Technology, Institute of Geology and Geophysics, Beijing 100049, China

Correspondence to: Bo Chen (bochen@csu.edu.cn)

Abstract. Building source models and performing forward calculations are fundamental for processing, analyzing, and interpreting geophysical data. However, there are rare open-source tools available that allow for both the flexible and interactive construction of source models and potential-field forward calculations. To address this gap, we developed a new Qt-based software called G&M3D 1.0, which supports interactive 3D model construction and provides accurate and efficient forward modelling. G&M3D 1.0 features two core functionalities: (1) constructing 3D gravity and magnetic source models and (2) calculating and visualizing their gravity/magnetic fields, as well as their gradient fields. In the 3D Modelling Module, rectangular prisms are used to approximate anomalous geological bodies, striking a balance between computational efficiency and geometric flexibility. Users can conveniently create 3D models with regular shapes, like spheres, cuboids, cylinders, and prismoids, each having variable densities or magnetic parameters. Complex structures can be modelled using the Irregular (Layer-Building) tool, which is especially suitable for stratigraphic or faulted formations. In addition, the Forward-Modelling Module allows for the rapid calculation, visualization, and saving of gravity anomalies, gravity gradients, total magnetic intensity, and magnetic gradients generated by the created 3D sources. To improve the efficiency of the gravity and magnetic forward calculations, the software employs a 2D discrete convolution algorithm. G&M3D 1.0 offers several significant advantages, including open-source accessibility, flexible interactive operations, an intuitive 3D modelling interface, efficient forward computation, and excellent file portability. As a demonstration of its capabilities, we utilized G&M3D 1.0 for forward gravity modelling over a salt dome at Vinton Dome in southern Louisiana, U.S., providing validation of its accuracy and practicality.

1 Introduction

Gravity and magnetic explorations are the most conventional geophysical methods, offering advantages such as simple construction, low costs, and efficient large-area data collection compared to other exploration techniques. Building forward source models and conducting forward calculations are fundamental for processing, analyzing, and interpreting gravity and

https://doi.org/10.5194/egusphere-2025-5357
Preprint. Discussion started: 23 January 2026

magnetic data (Blakely, 1996). However, there is still a lack of open-source tools with interactive interfaces that allow for flexible construction of source models and efficient forward modelling of the potential fields.

To estimate the gravitational or magnetic effects generated by anomalous masses, geophysicists often represent complex subsurface volumes or geological bodies as a combination of idealized sources with simple shapes (Blakely, 1996; Hinze et al., 2013). These shapes include spheres, cylinders, vertical laminas, horizontal laminas, prisms, and polyhedra. Most of these idealized sources can be easily integrated by volume and evaluated in closed analytical forms. Among these simple cells, the rectangular prism is particularly favoured for forward modelling and inversion, as it provides a straightforward way to approximate complicated anomalous sources and represents the total underground volume without gaps (Caratori Tontini et al., 2009; Li and Chouteau, 1998; Zhao et al., 2018).

Numerous early scholars have contributed to the closed formulas for gravity and magnetic anomalies caused by rectangular prisms (Bhattacharyya, 1964; Bhattacharyya and Navolio, 1976; Li and Chouteau, 1998; Nagy, 1966; Nagy et al., 2000; Okabe, 1979; Plouff, 1976). For example, Bhattacharyya (1964) presented formulas for the magnetic anomalies resulting from prism-shaped bodies with arbitrary polarization. Nagy (1966) derived a closed expression to calculate the gravitational attraction of a rectangular prism. Bhattacharyya and Navolio (1976) provided spectral expressions for the gravity and magnetic anomalies arising from irregular 3D sources by combining prisms. Later, Guo et al. (2004) introduced a new singularity-free calculation formula for the forward modelling of the magnetic field produced by a rectangular prism. Additionally, Luo and Yao (2007) optimized the theoretical magnetic calculation formula to improve its calculation efficiency.

A fine subdivision is often required to approximate anomalous bodies more precisely. However, when the subspace is finely subdivided, the repeated cumulative calculations can make the forward analysis time-consuming. To improve calculation efficiency, various algorithms have been developed for forward calculations of gravity and magnetic anomalies. For instance, Wu and Tian (2014) proposed a Gauss-fast Fourier transform (FFT) method for calculating potential fields in the Fourier domain. Zhang and Wong (2015) established a block-Toeplitz-Toeplitz-block (BTTB) structure using a discrete multi-layer model, then embedded the BTTB matrix into a block-cyclic-cyclic-block (BCCB) matrix by applying FFT in forward calculations. Additionally, Chen and Liu (2019) optimized the computation of the weight coefficient matrix and applied a 2D discrete convolution algorithm through block circulant extension (referred to as the BCE method) to calculate the gravity anomaly in the spatial domain. This method was later extended to calculate magnetic anomalies on undulating terrain (Qiang et al., 2019). Subsequently, Hogue et al. (2020) developed an open-source MATLAB code for evaluating gravity and magnetic kernels based on the BCE method. Recently, Yuan et al. (2022) advanced the BCE algorithm for magnetic forward modelling and inversion.

Significant progress has been made in the forward calculation of the potential fields; however, constructing a 3D anomalous model for testing forward or inversion algorithms can be complex and non-intuitive, especially when creating intricate irregular sources (Jessell et al., 2021). Various software packages are available for the computational synthesis of different geological models (de la Varga et al., 2019; Hassanzadeh et al., 2022; Jessell et al., 2014; Jessell et al., 2021; Pirot et al.,

https://doi.org/10.5194/egusphere-2025-5357
Preprint. Discussion started: 23 January 2026

2022; Wellmann et al., 2016). Nonetheless, there are rare open-source options that allow for the interactive creation of geologic bodies and efficient forward calculations of their potential fields. This study aims to develop free, open-source software that integrates flexible model construction with rapid forward calculations of potential fields.

C++ is a high-level programming language commonly used in high-performance computing and is particularly advantageous for numerical calculations, making it a popular choice in geophysical research. Qt, a powerful cross-platform C++ framework, is widely used for designing graphical user interface (GUI) applications across various platforms, including desktop, mobile, and embedded systems. It offers extensive development tools and libraries that facilitate the rapid creation of high-quality applications. For instance, Snopek and Casten (2006) developed the 3GRAINS software specifically for processing gravity and magnetic data.

In this study, we chose the rectangular prism as the primary cell to approximate the source volume. We then developed software called G&M3D 1.0 to construct 3D density and magnetic susceptibility models, as well as to forward calculate and visualize their gravity and magnetic fields using the Qt Creator framework and C++. The software includes the following functions: (1) interactively creating various geological models and assigning density contrasts or magnetization parameters; (2) performing fast and accurate forward calculations of gravity, gravity gradients, total magnetic intensity, and magnetic gradients. In addition, the models created with G&M3D 1.0 can be visualized and saved, and their density or magnetization distributions can be exported. The results from the forward modelling can also be flexibly visualized and saved.

The paper is organized as follows. Section 2 introduces the principles of gravity and magnetic forward calculation, as well as fast calculation strategies. In section 3, we describe the software workflow, focusing on how to create a source model and conduct forward modelling. Section 4 presents an example of applying G&M3D 1.0 to the real-world forward gravity modelling in Vinton Dome, southern Louisiana, U.S. The final section is the conclusions.

2 Forward Method

2.1 Forward modelling theory

As shown in Figure 1, a collection of rectangular prisms offers a straightforward method for approximating mass volume (Li and Chouteau, 1998). Each prism is assumed to have constant physical properties, such as density contrast or magnetization. For a rectangular prism whose dimensions are constrained as $[\xi_1, \xi_2]$, $[\eta_1, \eta_2]$, $[\zeta_1, \zeta_2]$ in the x, y, and z directions (Figure 1), the vertical component of the gravity attraction Δg and the gravity gradient components at the observation point $P(x, y, z_0)$ are given by (Li and Chouteau, 1998; Nagy et al., 2000),

$$\Delta g(x,y,z) = -G\rho \sum_{i=1}^{2}\sum_{j=1}^{2}\sum_{k=1}^{2} u_{ijk}\left[x_i \ln\left(r_{ijk}+y_j\right) + y_j \ln\left(r_{ijk}+x_i\right) - z_k \arctan\frac{x_i y_j}{z_k r_{ijk}}\right], \quad (1)$$

$$V_{zz}(x,y,z) = G\rho \sum_{i=1}^{2}\sum_{j=1}^{2}\sum_{k=1}^{2} u_{ijk} \arctan\frac{x_i y_j}{z_k r_{ijk}}, \quad (2)$$

https://doi.org/10.5194/egusphere-2025-5357
Preprint. Discussion started: 23 January 2026

$$V_{xx}(x,y,z) = G\rho \sum_{i=1}^{2}\sum_{j=1}^{2}\sum_{k=1}^{2} u_{ijk}\arctan\frac{y_j z_k}{x_i r_{ijk}}, \tag{3}$$

$$V_{yy}(x,y,z) = G\rho \sum_{i=1}^{2}\sum_{j=1}^{2}\sum_{k=1}^{2} u_{ijk}\arctan\frac{x_i z_k}{y_j r_{ijk}}, \tag{4}$$

$$V_{xz}(x,y,z) = -G\rho \sum_{i=1}^{2}\sum_{j=1}^{2}\sum_{k=1}^{2} u_{ijk}\ln(r_{ijk} + y_j), \tag{5}$$

$$V_{yz}(x,y,z) = -G\rho \sum_{i=1}^{2}\sum_{j=1}^{2}\sum_{k=1}^{2} u_{ijk}\ln(r_{ijk} + x_i), \tag{6}$$

$$V_{xy}(x,y,z) = -G\rho \sum_{i=1}^{2}\sum_{j=1}^{2}\sum_{k=1}^{2} u_{ijk}\ln(r_{ijk} + z_k), \tag{7}$$

where G is the universal gravitational constant (6.672×10^{-11} Nm^2/kg^2), ρ is the density contrast of the rectangular prism, $x_i = x - \xi_i$, $y_j = y - \eta_j$, $z_k = z_0 - \zeta_k$, $r_{ijk} = \sqrt{{x_i}^2 + {y_j}^2 + {z_k}^2}$, and $u_{ijk} = (-1)^i(-1)^j(-1)^k$. The z-axis is taken to be positive downward.

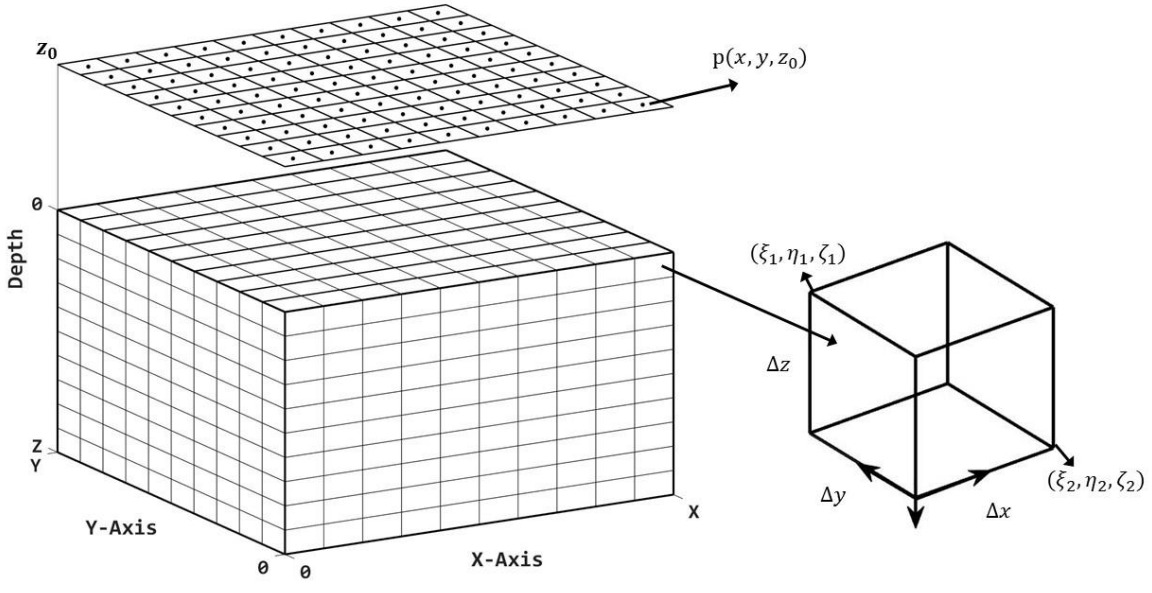

Figure 1: Division schematic diagram of the source region and observation points.

The three components of the magnetic field anomaly (B_x, B_y, B_z) and its gradient tensors due to the prism at the observation point $P(x, y, z_0)$ are provided by (Gao, 2019; Luo and Yao, 2007),

https://doi.org/10.5194/egusphere-2025-5357
Preprint. Discussion started: 23 January 2026

$$B_x(x,y,z) = \frac{\mu_0 M}{4\pi}\sum_{i=1}^{2}\sum_{j=1}^{2}\sum_{k=1}^{2} u_{ijk}\left[-k_1 arctan\frac{y_j z_k}{x_i r_{ijk}} + k_2 \ln(r_{ijk}+z_k) + k_3 \ln(r_{ijk}+y_j)\right], \quad (8)$$

$$B_y(x,y,z) = \frac{\mu_0 M}{4\pi}\sum_{i=1}^{2}\sum_{j=1}^{2}\sum_{k=1}^{2} u_{ijk}\left[k_1 \ln(r_{ijk}+z_k) - k_2 arctan\frac{x_i z_k}{y_j r_{ijk}} + k_3 \ln(r_{ijk}+x_i)\right], \quad (9)$$

$$B_z(x,y,z) = \frac{\mu_0 M}{4\pi}\sum_{i=1}^{2}\sum_{j=1}^{2}\sum_{k=1}^{2} u_{ijk}\left[k_1 \ln(r_{ijk}+y_j) + k_2 \ln(r_{ijk}+x_i) - k_3 arctan\frac{x_i y_j}{z_k r_{ijk}}\right], \quad (10)$$

$$B_{xx}(x,y,z) = -\frac{\mu_0 M}{4\pi}\sum_{i=1}^{2}\sum_{j=1}^{2}\sum_{k=1}^{2} u_{ijk}\left[k_1 \frac{y_j z_k (r_{ijk}{}^2 + x_i{}^2)}{(x_i{}^2 + z_k{}^2)(x_i{}^2 + y_j{}^2) r_{ijk}} + k_2 \frac{x_i}{r_{ijk}(r_{ijk}+z_k)} + k_3 \frac{x_i}{r_{ijk}(r_{ijk}+y_j)}\right], \quad (11)$$

$$B_{yy}(x,y,z) = -\frac{\mu_0 M}{4\pi}\sum_{i=1}^{2}\sum_{j=1}^{2}\sum_{k=1}^{2} u_{ijk}\left[k_1 \frac{y_j}{r_{ijk}(r_{ijk}+z_k)} + k_2 \frac{x_i z_k (r_{ijk}{}^2 + y_j{}^2)}{(y_j{}^2 + z_k{}^2)(x_i{}^2 + y_j{}^2) r_{ijk}} + k_3 \frac{y_j}{r_{ijk}(r_{ijk}+x_i)}\right], \quad (12)$$

$$B_{zz}(x,y,z) = -\frac{\mu_0 M}{4\pi}\sum_{i=1}^{2}\sum_{j=1}^{2}\sum_{k=1}^{2} u_{ijk}\left[k_1 \frac{z_k}{r_{ijk}(r_{ijk}+y_j)} + k_2 \frac{z_k}{r_{ijk}(r_{ijk}+x_i)} + k_3 \frac{x_i y_j (r_{ijk}{}^2 + z_k{}^2)}{(x_i{}^2 + z_k{}^2)(y_j{}^2 + z_k{}^2) r_{ijk}}\right], \quad (13)$$

$$B_{xy}(x,y,z) = B_{yx}(x,y,z) = -\frac{\mu_0 M}{4\pi}\sum_{i=1}^{2}\sum_{j=1}^{2}\sum_{k=1}^{2} u_{ijk}\left[k_1 \frac{x_i}{r_{ijk}(r_{ijk}+z_k)} + k_2 \frac{y_j}{r_{ijk}(r_{ijk}+z_k)} + k_3 \frac{1}{r_{ijk}}\right], \quad (14)$$

$$B_{yz}(x,y,z) = B_{zy}(x,y,z) = -\frac{\mu_0 M}{4\pi}\sum_{i=1}^{2}\sum_{j=1}^{2}\sum_{k=1}^{2} u_{ijk}\left[k_1 \frac{1}{r_{ijk}} + k_2 \frac{y_j}{r_{ijk}(r_{ijk}+x_i)} + k_3 \frac{z_k}{r_{ijk}(r_{ijk}+x_i)}\right], \quad (15)$$

$$B_{xz}(x,y,z) = B_{zx}(x,y,z) = -\frac{\mu_0 M}{4\pi}\sum_{i=1}^{2}\sum_{j=1}^{2}\sum_{k=1}^{2} u_{ijk}\left[k_1 \frac{x_i}{r_{ijk}(r_{ijk}+y_j)} + k_2 \frac{1}{r_{ijk}} + k_3 \frac{z_k}{r_{ijk}(r_{ijk}+y_j)}\right], \quad (16)$$

where M is the induced magnetization intensity of the rectangular prism with the inclination (I') and declination (D'), $k_1 = cosI'cosD'$, $k_2 = cosI'sinD'$, $k_3 = sinI'$, $\mu_0 = 4\pi \times 10^{-7}$ H/m is the magnetic permeability of the vacuum.

Suppose the magnetic anomaly caused by a magnetic body is small compared to the main magnetic field. The scalar magnitude of the magnetic field anomalies can be approximately calculated by projecting the components of the anomalous field in the direction of the Earth's main field (Hinze et al., 2013; Plouff, 1976). As a result, the total magnetic intensity anomaly ΔT and its gradients ($\Delta T_x, \Delta T_x, \Delta T_z$) from the source can be approximated by (Hinze et al., 2013),

https://doi.org/10.5194/egusphere-2025-5357
Preprint. Discussion started: 23 January 2026

$$\Delta T = B_x cosIcosD + B_y cosIsinD + B_z sinI, \quad (17)$$

$$\Delta T_x = B_{xx} cosIcosD + B_{yx} cosIsinD + B_{zx} sinI, \quad (18)$$

$$\Delta T_y = B_{xy} cosIcosD + B_{yy} cosIsinD + B_{zy} sinI, \quad (19)$$

$$\Delta T_z = B_{xz} cosIcosD + B_{yz} cosIsinD + B_{zz} sinI, \quad (20)$$

where I and D are the inclination and declination of the Earth's geomagnetic field at the observation point.

2.2 Fast forward modelling method

In G&M3D 1.0, we define a source region with the range $[0,\ X]$, $[0,\ Y]$, and $[0,\ Z]$ in the x, y, and z axes, respectively. The source space is divided into $N \times M \times L$ prisms, each with dimensions of $\Delta x \times \Delta y \times \Delta z$. These prisms are labeled as (a, b, c), with their dimensions limited to $[\xi_{1,a} = (a-1)\Delta x,\ \xi_{2,a} = a\Delta x]$, $[\eta_{1,b} = (b-1)\Delta y,\ \eta_{2,b} = b\Delta y]$, $[\zeta_{1,c} = (c-1)\Delta z,\ \zeta_{2,c} = c\Delta z]$, where $a = 1,2 \dots, N;\ b = 1, \dots, M; c = 1, \dots, L$.

The observation points (x_n, y_m), where $x_n = (n-0.5)\Delta x, n = 1, \dots, N; y_m = (m-0.5)\Delta y, m = 1, \dots, M$, are distributed at the horizontal surface z_0 at regular intervals, aligned with the prism centers, as shown in Figure 1. The gravity/magnetic fields at the observation $P(x_n, y_m, z_0)$ can be calculated by summing the contributions from all prisms within the source region, which can be written as

$$\mathrm{g}(x_n, y_m, z_0) = \sum_{c=1}^{L} \left[\sum_{a=1}^{N} \sum_{b=1}^{M} f(a,b,c) \times t(x_n, y_m, z_0; a, b, c) \right], \quad (21)$$

where f is the density or magnetization value corresponding to the prism (a, b, c), $t(x_n, y_m, z_0; a, b, c)$ is the field response at the observation point (x_n, y_m, z_0) due to the prism (a, b, c) with unit density or magnetization. This field response can be calculated using any of Eqs. (1) to (16), which represent the kernel or sensitivity function.

Thanks to Eq. (21), the gravity/magnetic field at all observation points can be presented in matrix-vector form as follows,

$$\mathbf{g} = \mathbf{K} \cdot \boldsymbol{f}, \quad (22)$$

where $\mathbf{g}$ is the field vector, $\boldsymbol{f}$ is the density/magnetization parameter vector, $\mathbf{K}$ represents the kernel matrix (or sensitivity matrix) with dimension $(N \times M) \times (N \times M \times L)$, which is classified as a Block-Toeplitz Toeplitz-Block (BTTB) matrix.

The forward calculations described in Eq. (22) can be time-consuming, particularly when the source space is large and finely discretized. In this study, we apply a 2D discrete convolution algorithm using block circulant extension (BCE) (Chen and Liu, 2019) to optimize the forward calculations. In G&M3D 1.0, we conduct forward calculations of potential fields layer by layer along the z direction using the BCE algorithm. The procedure for the BCE algorithm (Chen and Liu, 2019) is as follows.

First, the density/magnetization values of all the prisms are stored in a 3-D matrix $\boldsymbol{E}$ of size $N \times M \times L$. For any given layer (e.g., the c^{th} layer, $c = 1, \dots, L$), the parameter vector is defined as $\boldsymbol{f} = \boldsymbol{E}(1{:}N, 1{:}M, c)$. A null parameter vector $\boldsymbol{f}$ (where all elements equal zero) indicates that the prisms in the c^{th} layer make no contribution to the observed field. For non-zero cases, the matrix $\boldsymbol{f}$ is extended with zeros to form an extended parameter matrix $\mathbf{F}$,

https://doi.org/10.5194/egusphere-2025-5357
Preprint. Discussion started: 23 January 2026

$$\mathbf{F} = \begin{bmatrix} \boldsymbol{f} & \mathbf{0}_{N\times M} \\ \mathbf{0}_{N\times M} & \mathbf{0}_{N\times M} \end{bmatrix}. \tag{23}$$

Next, the observation range is extended along the negative direction of the x-axis and y-axis from $[0, X]$, $[0, Y]$ to $[-X + \Delta x, X]$, $[-Y + \Delta y, Y]$, as shown in Figure 2. We then compute the field effects generated by the prism $(a = 1, b = 1, c)$ (dimensions limited as $[\xi_1 = 0, \xi_2 = \Delta x]$, $[\eta_1 = 0, \eta_2 = \Delta y]$, $[\zeta_1 = (c-1)\Delta z,\ \zeta_2 = c\Delta z]$) at all observations in the extended area. This results in an extended response matrix $\mathbf{T}$ with a size of $(2N-1) \times (2M-1)$ for the c^{th} layer,

$$\mathbf{T} = \begin{bmatrix} t_{1,1} & \cdots & t_{1,2M-1} \\ \vdots & t_{n',m'} & \vdots \\ t_{2N-1,1} & \cdots & t_{2N-1,2M-1} \end{bmatrix}, \tag{24}$$

where $t_{n',m'}$ $(n' = 1,2,\ldots,2N-1; m' = 1,2,\ldots,2M-1)$ is the field response at the observation $P(x_{n'}, y_{m'}, z_0)$ where $x_{n'} = (n' - N + 0.5)\Delta x$, $y_{m'} = (m' - M + 0.5)\Delta y$, which is calculated using Eqs. (1) to (16) with unit density or induced magnetization intensity (namely, $\rho = 1$, $M = 1$).

We extend $\mathbf{T}$ by zeros along the top and the left margins, as shown in Figure 2. This creates a matrix $\mathbf{T_0}$ with a size of $2N \times 2M$,

$$\mathbf{T_0} = \begin{bmatrix} 0 & \mathbf{0}_{1\times(2M-1)} \\ \mathbf{0}_{(2N-1)\times 1} & \mathbf{T} \end{bmatrix}, \tag{25}$$

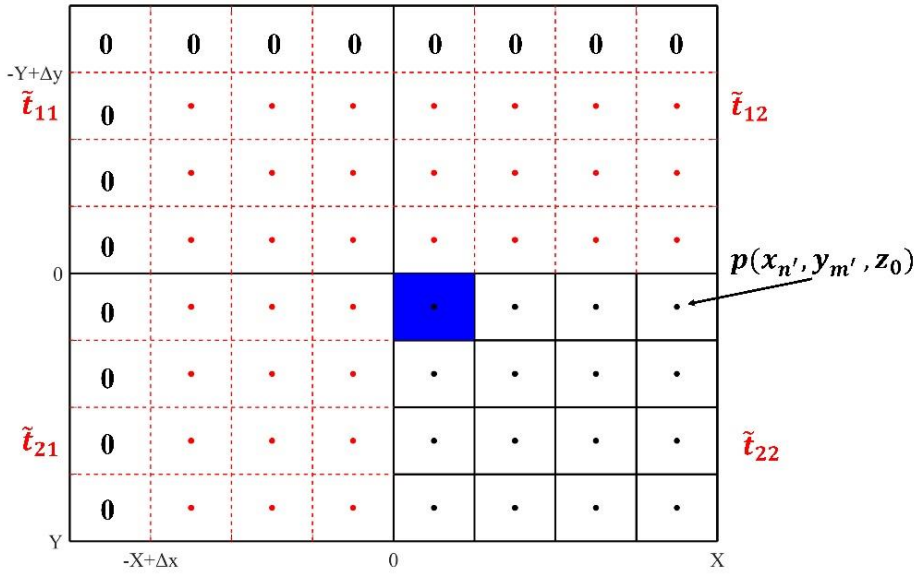

Figure 2: The sketch map shows the extended observation points and source region for the BCE method. The prism (1, 1) is marked in blue. A single-layer model consisting of 4×4 prisms is taken as an example.

The matrix $\mathbf{T_0}$ in Eq. (25) can then be rewritten into four $N \times M$ submatrices as,

$$\mathbf{T_0} = \begin{bmatrix} \tilde{\boldsymbol{t}}_{11} & \tilde{\boldsymbol{t}}_{12} \\ \tilde{\boldsymbol{t}}_{21} & \tilde{\boldsymbol{t}}_{22} \end{bmatrix}, \tag{26}$$

https://doi.org/10.5194/egusphere-2025-5357
Preprint. Discussion started: 23 January 2026

By reordering the submatrices in Eq. (24), we get

$$\mathbf{C} = \begin{bmatrix} \tilde{\boldsymbol{t}}_{22} & \tilde{\boldsymbol{t}}_{21} \\ \tilde{\boldsymbol{t}}_{12} & \tilde{\boldsymbol{t}}_{11} \end{bmatrix}. \tag{27}$$

The matrix $\mathbf{C}$ in Eq. (27) is identified as a Block-Cyclic-Cyclic-Block (BCCB) matrix. The 2D discrete convolution of this matrix with the extended parameter matrix $\mathbf{F}$ can be efficiently computed using the fast Fourier transform (Chen and Liu, 2019; Vogel, 2002) as follows,

$$\tilde{\mathbf{C}} = fft2(\mathbf{C}), \tag{28}$$

$$\tilde{\mathbf{F}} = fft2(\mathbf{F}), \tag{29}$$

$$\tilde{\mathbf{G}} = \tilde{\mathbf{C}} .* \tilde{\mathbf{F}}, \tag{30}$$

$$\mathbf{G} = ifft2(\tilde{\mathbf{G}}), \tag{31}$$

$$\mathbf{G}_c = \mathbf{G}(1{:}N, 1{:}M), \tag{32}$$

where $fft2$ is the 2D fast Fourier transform, and $ifft2$ denotes the 2D inverse fast Fourier transform. The symbol $.*$ represents the dot multiplication operator. $\mathbf{G}_c$ is the resulting field at the observations generated by the anomalous prisms in the c^{th} layer.

Repeat these steps for each layer, and the total field $\mathbf{g}$ at all observations is obtained by,

$$\mathbf{g} = \sum_{c=1}^{L} \boldsymbol{G}_c, \tag{33}$$

From a programming perspective, we implemented several strategies to enhance computational efficiency in G&M3D 1.0.

Strategy 1. We took advantage of the fast matrix operation in Qt to optimize the forward calculations in G&M3D 1.0. We pre-constructed two new matrices $\boldsymbol{X}_i$ and $\boldsymbol{Y}_j$ with sizes of $(2N-1) \times (2M-1)$,

$$\boldsymbol{X}_i = \begin{bmatrix} x_1 & \cdots & x_1 \\ \vdots & x_{n'} & \vdots \\ x_{2N-1} & \cdots & x_{2N-1} \end{bmatrix} - \xi_i \mathbf{I}, \tag{34}$$

$$\boldsymbol{Y}_j = \begin{bmatrix} y_1 & \cdots & y_{2M-1} \\ \vdots & y_{m'} & \vdots \\ y_1 & \cdots & y_{2M-1} \end{bmatrix} - \eta_j \mathbf{I}, \tag{35}$$

where $i, j = 1, 2$, $x_{n'} = (n' - N + 0.5)\Delta x$, $y_{m'} = (m' - M + 0.5)\Delta y$, $(n' = 1,2,\ldots,2N-1; m' = 1,2,\ldots,2M-1)$, $\xi_1 = 0$, $\xi_2 = \Delta x$, $\eta_1 = 0$, $\eta_2 = \Delta y$. $\mathbf{I}$ is an all-ones matrix. Thanks to the Eqs. (32) to (33), we can substitute the matrices $\boldsymbol{X}_i$ and $\boldsymbol{Y}_j$ to x_i and y_j in any of the Eqs (1) to (16). This allows the extended response matrix $\mathbf{T}$ at all observations to be computed by a single dot product in Qt, rather than relying on a large number of cyclic calculations.

Strategy 2. Since the kernel matrices for gravity and magnetic components under vertical magnetization are symmetric (Hogue et al., 2020), we only calculate the submatrix $\tilde{\boldsymbol{t}}_{22}$ in $\mathbf{C}$ (Eq. (27)) for these cases. The other three submatrices ($\tilde{\boldsymbol{t}}_{11}$, $\tilde{\boldsymbol{t}}_{12}$, $\tilde{\boldsymbol{t}}_{21}$) can be derived from $\tilde{\boldsymbol{t}}_{22}$, because they share the same value or have the opposite sign as $\tilde{\boldsymbol{t}}_{22}$. This strategy results in a higher efficiency for forward calculations of gravity anomalies, gravity gradient tensor, and magnetic components with vertical magnetization compared to those for the magnetic field with non-vertical magnetization. As we know, the forward

https://doi.org/10.5194/egusphere-2025-5357
Preprint. Discussion started: 23 January 2026

calculations of magnetic fields depend on the declination and inclination of the sources. If the models in the source region have varying declinations or inclinations, we classify these models by their declinations or inclinations and perform forward calculations of each category separately.

2.3 Synthetic model tests

To verify the efficiency of the forward calculation in G&M3D 1.0, we design a synthetic model with known density and magnetization for gravity and magnetic forward modeling. The model region extends from 0 m to 500 hm in the x, y, and z axes. It consists of an anomalous block with a density contrast of 1 g/cm^3 and an induced magnetization of 1 A/m. The center of the anomalous block is located at (250, 250, 250) hm with a size of 250×250×200 hm^3.

We examine the computation time for gravity and magnetic forward calculations using three different grid sizes, i.e., 50×50×50, 100×100×100, and 200×200×200. This means that the source region is divided into a combination of prisms with grid intervals of 10 hm, 5 hm, and 2.5 hm, respectively. The absolute computation time for the forward calculation of the gravity and magnetic fields is summarized in Table 1.

Table 1: The statistics of the absolute consumption time for forward computations of the gravity and magnetic fields with three different grid numbers.

Grid interval (hm) / Grid number	Computation time (s)		
	Gravity components	Magnetic components for vertical magnetization	Magnetic components for non-vertical magnetization
10.0/50×50×50	0.167	0.153	0.465
5.0/100×100×100	1.323	1.455	4.054
2.5/200×200×200	10.157	9.684	34.371

Note. All the tests were carried out on a desktop with an AMD Ryzen 7 3700X CPU and 32 GB of memory. No parallel computational strategy is used.

Table 1 presents that the computation time increases significantly with the increase in grid numbers. Note that the output results of the gravity calculation in Table 1 consist of 7 components, i.e., $\Delta g, V_{zz}, V_{xx}, V_{yy}, V_{xz}, V_{yz}, V_{xy}$, and the results of magnetic forward modeling include 13 components (i.e., $B_x, B_y, B_z, B_{xx}, B_{yy}, B_{zz}, B_{xy}, B_{xz}, B_{yz}, \Delta T, \Delta T_x, \Delta T_x, \Delta T_z$). Due to the implementation of Strategy 2, which decouples the computation of vertically and non-vertically magnetized models, the efficiency of forward modeling has improved significantly. In a 200×200×200 grid case, the computation time was reduced by 71.83% (34.371 vs. 9.684). These tests demonstrate that G&M3D 1.0 is a high-speed tool for forward calculations of the gravity and magnetic fields. It is worth noting that the layers with non-zero density/magnetization occupy 40% of the total layers in the z direction in these tests. The forward calculation will be faster if the anomalous body's vertical dimension is reduced, but it will require more time if the vertical dimension exceeds the current size.

https://doi.org/10.5194/egusphere-2025-5357
Preprint. Discussion started: 23 January 2026

3 The framework and functions of G&M3D

In this section, we introduce the functions and operational procedures of G&M3D 1.0. This software consists of two main modules: (1) building 3D density or magnetic source models, and (2) calculating the gravity or magnetic fields produced by these source models. The workflow of G&M3D 1.0 is shown in Figure 3.

When users open G&M3D 1.0 and enter the start interface (Figure 3), they can access the 3D-Modeling module to create a new source model by clicking the button **Create Model**, or they can input an existing model data file to conduct gravity or magnetic forward calculations through the Forward-Modeling module by clicking the button **Input Model**.

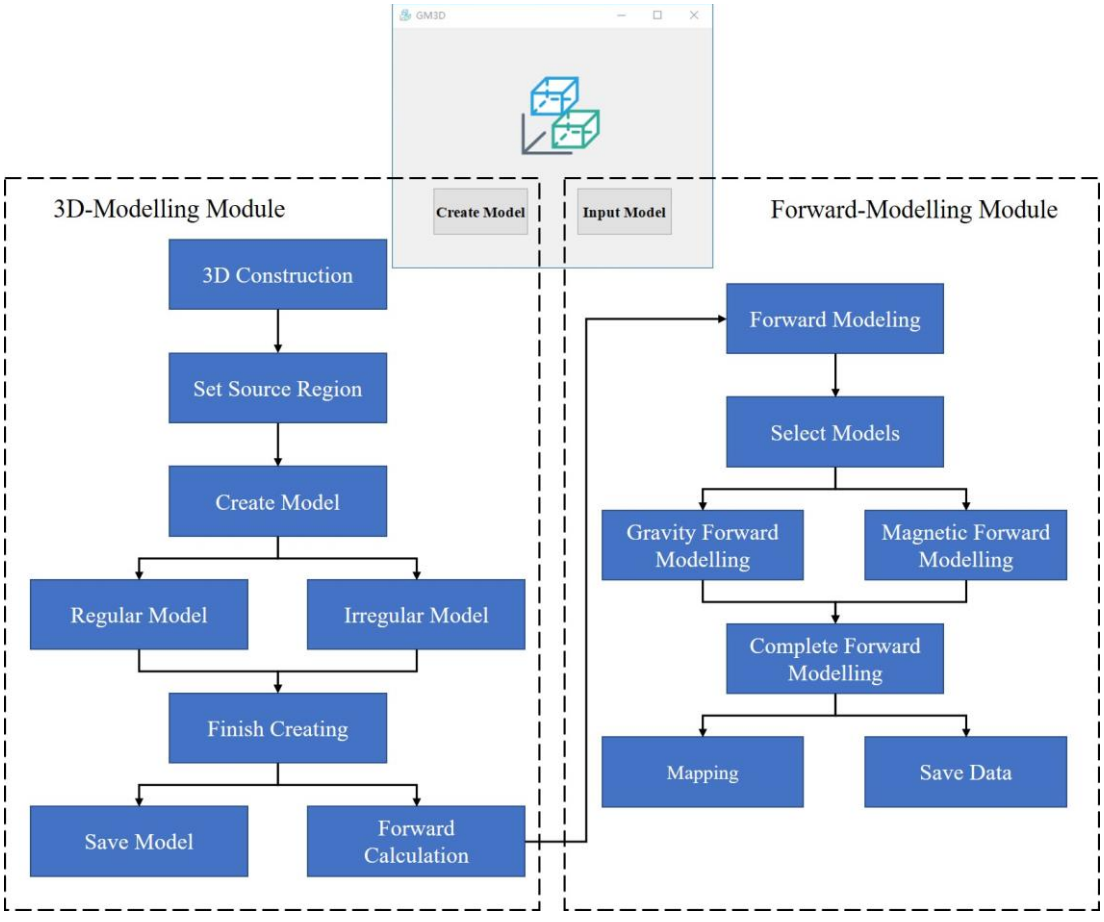

Figure 3: Workflow in G&M3D 1.0 and G&M3D 1.0 initial interface.

The main interface of the Modelling module is shown in Figure 4a. By default, G&M3D 1.0 generates an initial source region (Figure 4b). To customize this for their needs, users should first set the source region by clicking the “Settings” button in the operation area of the main interface. In the pop-up window for the Setting Field (Figure 4b), users can configure the basic parameters that define the source region, including the source range, mesh interval, and length unit. The supported

https://doi.org/10.5194/egusphere-2025-5357
Preprint. Discussion started: 23 January 2026

length units are meters (m), hectometers (hm), and kilometers (km), which allow for multi-scale forward modeling simulations.

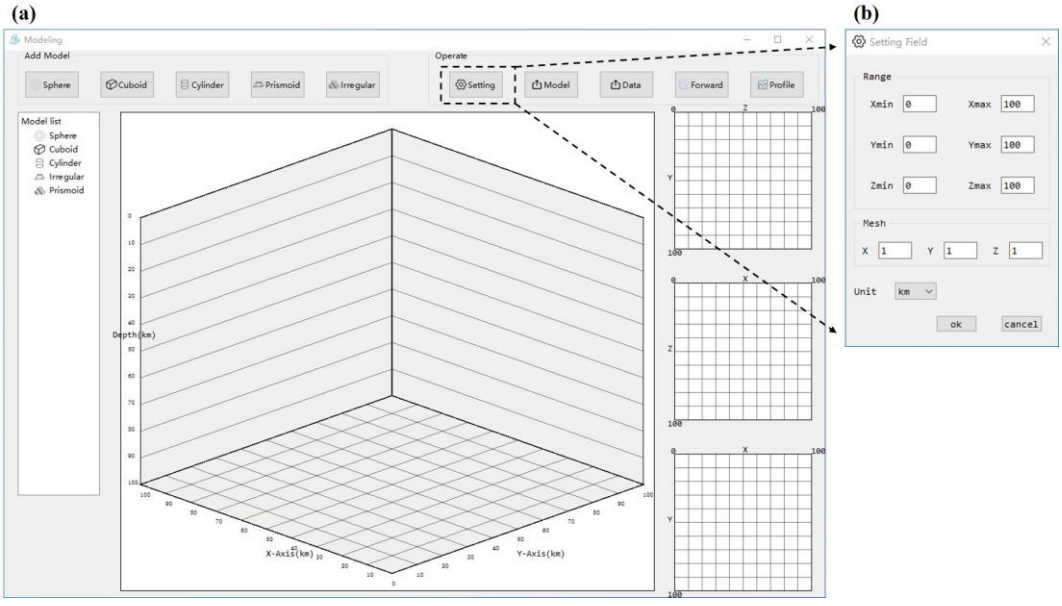

Figure 4: (a)Interface of the Modelling Module. The top functional area contains modelling of different shapes on the left and various action buttons on the right. The middle workspace is used to display the created models (the 2D floor plan is shown in three areas on the right), and the list of models is shown on the left. (b) Setting Field window. The default initial source region configuration is in the Setting Field window.

After that, users can select one of the tools on the "Add Model" panel to create source models. G&M3D 1.0 supports sequential creation of multiple anomaly bodies, with all generated models automatically listed in the "Model List" section. To ensure modeling flexibility and operational efficiency, right-click functionality is provided for existing anomalies, allowing users to modify and delete them. The modification process uses the same intuitive interface as the creation process, making it just as easy to change models as it is to create them.

The following section explains the construction methods for regular and irregular models, which differ in their modeling approaches. However, both types share the same parameter configurations for gravity and magnetic properties. As shown in the "Property" panel of Figure 5, only four parameters need to be specified: density contrast, induced magnetization intensity, magnetic declination, and magnetic inclination.

G&M3D 1.0 provides four tools for creating regular-shaped bodies: **Sphere**, **Cuboid**, **Cylinder**, and **Prismoid**. Figure 5 displays the parameter input interfaces for each tool. (1) **Sphere**: This tool requires the radius and the coordinates of the sphere's center. (2) **Cuboid**: Users must input the geometric centre coordinates and the extension lengths along three orthogonal axes. (3) **Cylinder**: Four key parameters are needed to define a cylinder, including the trend direction, extension length, cross-sectional radius, and section centre coordinates. (4) **Prismoid**: This geometry is defined by three sets of spatial parameters: the x-coordinates of its four *y*-parallel edges, the *y*-coordinates of its four *x*-parallel edges, and the *z*-values for

https://doi.org/10.5194/egusphere-2025-5357
Preprint. Discussion started: 23 January 2026

its top and bottom planes. To enhance modelling flexibility, the "Direction" parameter specifies the normal vector orientation of the bounding planes relative to the coordinate axes. The **Prismoid** tool maintains strict geometric validity by enforcing essential constraints: the *x*-coordinates must be monotonically increasing ($x1 < x2$), as well as the *y*-coordinates ($y1 < y2$), ensuring proper spatial relationships for meaningful prism construction. All models require input of either density contrast or magnetization. Additionally, the "Mark" panel allows users to customize both the model's name and display colour according to their preferences. As an example, we created two models using each tool, resulting in a total of eight models, which are presented in Figure 6.

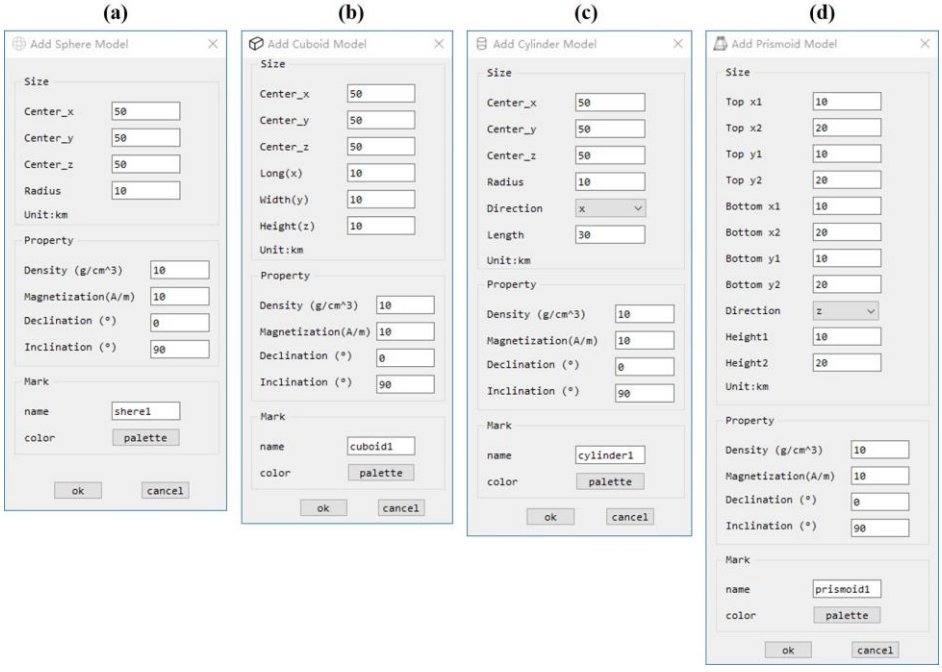

Figure 5: Parameter input interfaces for the four regular tools, including (a) Sphere, (b) Cuboid, (c) Cylinder, and (d) Prismoid.

https://doi.org/10.5194/egusphere-2025-5357
Preprint. Discussion started: 23 January 2026

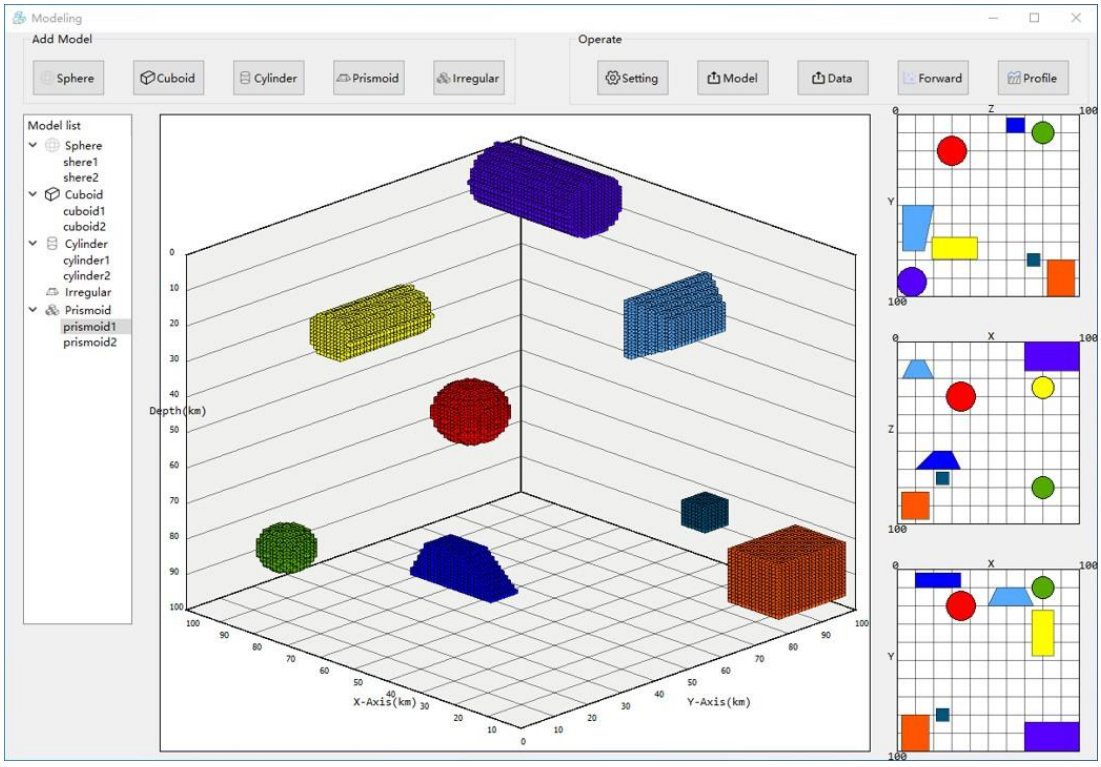

Figure 6: Illustration of regular modelling tools showing eight anomalous bodies.

G&M3D 1.0 features an **Irregular** tool that enables users to create irregular models, as shown in Figure 7. With the **Irregular** tool, users can accurately construct irregularly shaped bodies by interactively drawing their spatial boundaries across multiple layers. This layer-stacking method allows for the reconstruction of complex volumetric shapes that cannot be represented using conventional geometric primitives. G&M3D 1.0 automatically generates a set of prisms that fit within the limits defined by users in one layer, extending along the *x*, *y*, or *z* direction. To enhance operational efficiency, the software employs a dual-mode: Build Mode for creating anomalous prismatic units, and Erase Mode for removing existing anomalous units. These complementary modes work in tandem to minimize operational errors, effectively eliminating the need for complete rebuilds in case of mistakes. To maximize operational flexibility while avoiding redundant constraints, both modes maintain identical workflows and interaction processes.

https://doi.org/10.5194/egusphere-2025-5357
Preprint. Discussion started: 23 January 2026

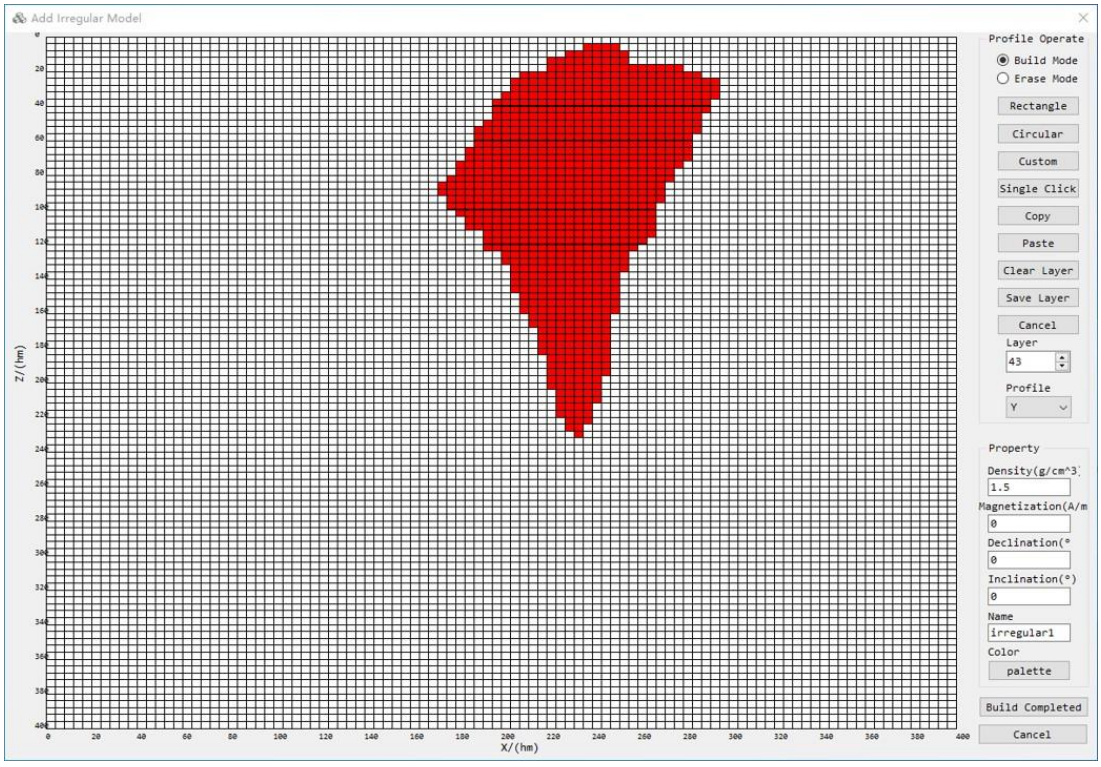

Figure 7: Interface of the Irregular tool. The main area is used to delineate the boundaries of the anomalous bodies. Right panels contain functional zones and parameter setting areas. Build Completed and Cancel buttons are used to finalize or abort the entire irregular modelling process, while all other functions only operate on the current layer. A sulphide deposit with a density contrast of 1.5 g/cm3 is an example, adapted according to Thomas (1997).

In the **Irregular** tool, G&M3D 1.0 offers four drawing modes: **Rectangle**, **Circular**, **Custom**, and **Single Click**. The modeling process uses a standardized left-click operation across all modes. Users press and hold the mouse button to activate a real-time visual preview of the modeling area, and release it to confirm and finalize the operation. In the **Custom** mode, users can draw any closed curve to define the boundary of the anomalous body, allowing automatically formed prisms to fit the limits more accurately with gradual sketching. To enhance workflow efficiency, G&M3D 1.0 includes **Copy** and **Paste** functionality for layers. Once users have finalized the geometric modeling and parameter settings (via the unified Property panel, consistent with regular modeling tools) for the current layer, they must manually save the layer data using the **Save Layer** option. After completing the model construction for all target layers, users can execute the **Build Completed** command to finalize and save the complete dataset. An example of constructing an irregular sulfide deposit model is provided in Figure 8.

https://doi.org/10.5194/egusphere-2025-5357
Preprint. Discussion started: 23 January 2026

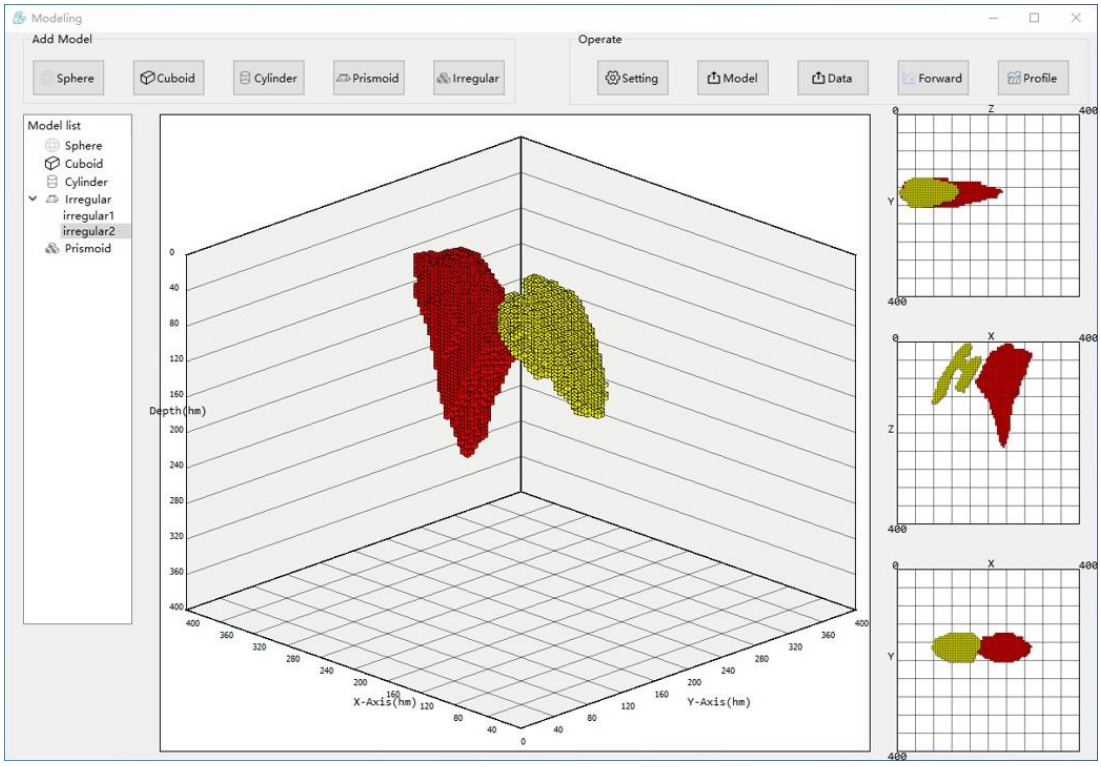

Figure 8: A sulphide deposit created by the Irregular tool.

Once all the models are created, the model data and the spatial distribution of density/magnetization within the source region can be exported. G&M3D 1.0 offers two distinct data export ways. The **Model** tool allows for the export of .bin files for internal use, while the **Data** tool generates .txt files to ensure data portability and compatibility with external applications across different platforms. This design not only facilitates the segmentation of workflows between building source models and forward modeling tasks, potentially assigned to different operators, but also enhances operational flexibility throughout the gravity and magnetic data processing workflow. The binary .bin format efficiently retains comprehensive parametric data, while the text-based .txt export adheres to standardized formatting specifications to facilitate interdisciplinary data exchange.

G&M3D 1.0 provides two methods for implementing forward modeling. Users can either initiate the computation through the **Forward** tool found in the "Operate" panel (Figure 4) to build source models and perform forward modeling within a unified project environment or directly import the pre-constructed models into the Forward-Modeling module using the **Input Model** option (Figure 3). Figure 9 shows the main interface of the Forward-Modeling module. To conduct forward calculations, users must first select the desired source models by checking the corresponding boxes in the "Model List" panel. Once the models are selected, users can start selecting the forward modeling process by clicking the **Forwarding** buttons, which will open the Forwarding Model interface (Figure 9b). Users are then required to configure the observation parameters. To accommodate mobile platform-based gravity and magnetic surveys, users can specify the observation height and optionally add noise to the data. After configuring these settings, clicking the **ok** button will execute the forward calculation.

https://doi.org/10.5194/egusphere-2025-5357
Preprint. Discussion started: 23 January 2026

Upon completion of the forward calculations, G&M3D 1.0 automatically generates a pseudocolor plot of the results. Users can switch to different data sets using the drop-down box in the Forward-Modeling interface. The results from the forward modeling can be viewed in G&M3D 1.0 or exported as a dataset by clicking the **Save Data** button.

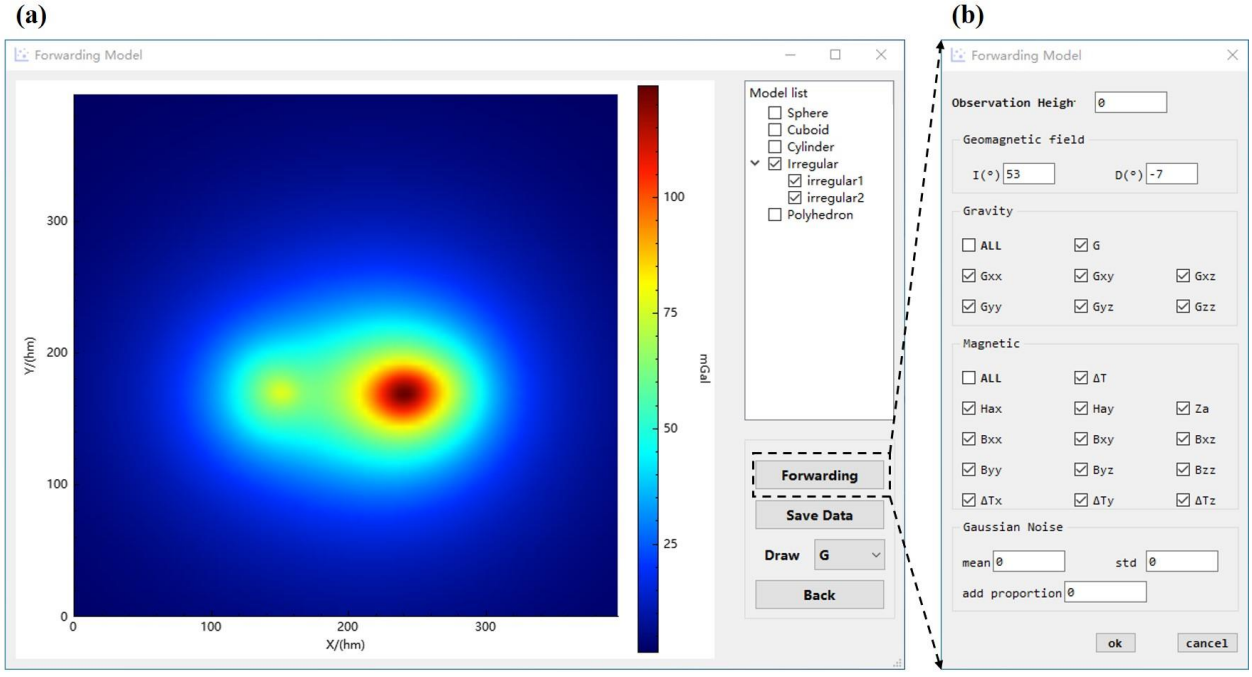

Figure 9: (a)Interface of the Forward-Modelling module. The left workspace is used to visualize the gravity/magnetic field. The upper right area shows the model list, and different models can be selected for forward calculation. The functional control area is located in the lower right section. A sulphide deposit is shown as an example, which is adapted according to Thomas (1997). (b)Parameter input pop-up window for Gravity forward modelling, Magnetic forward modelling. A certain proportion of Gaussian noise can be added to the field values to simulate errors. Mag-Inclination and Mag-Declination correspond to the inclination (I) and declination (D) of the Earth's geomagnetic field in Eqs. (17) to (20). Users can freely select the field category to be calculated.

4 Application

The 3D modeling and forward calculations of the gravity and magnetic fields in G&M3D 1.0 provide practical tools for potential data analysis and interpretation. It aids research on both forward modeling and inversion algorithms for gravity and magnetic data. Researchers often conduct synthetic model experiments to test the feasibility of their algorithms and assess parameter sensitivity. With G&M3D 1.0, they can easily create numerous artificial density or susceptibility models and quickly obtain the gravity/magnetic data generated by these models. Moreover, G&M3D 1.0 serves as a practical educational resource for teaching geophysics, particularly for beginners in gravity and magnetic exploration. Educators and students can utilize G&M3D 1.0 to construct simplified geophysical models, enabling them to explore the principles of the potential fields through interactive visualization and analysis.

https://doi.org/10.5194/egusphere-2025-5357
Preprint. Discussion started: 23 January 2026

To illustrate the usage of G&M3D 1.0, we carry out a gravity modeling analysis of a distinctive salt dome as an example. This salt dome model is based on available seismic and drill-hole data from Vinton Dome in southern Louisiana (Ennen, 2012). It features a caprock with positive-density at depths ranging from 160 to 760 m, alongside a negative-density salt volume located deeper. In the study by Ennen (2012), gravity gradients produced by this salt dome model were calculated and compared to observed airborne gravity gradient data to identify potential oil signals. As highlighted in Ennen's research, constructing such an irregular density model for a salt dome is a labor-intensive process.

In this example, we utilize the salt dome model described by Ennen (2012) to demonstrate the 3-D modeling and forward calculations of gravity gradients using G&M3D 1.0. According to this study, the source space is divided into 66 × 45 × 28 prisms with a size of 100×100×100 m. The density anomaly of the salt dome varies in geometry at different depths, with differing density contrasts, as presented in Table 2.

Table 2: Density distribution of the salt dome model along the depth

Anomalous body number	Depth range of sources /m	Density contrast (kg/m³)
1	60-160	575
2	160-260	575
3	260-360	400
4	360-460	400
5	460-760	50
6	760-1060	-20
7	1060-1360	-50
8	1360-1660	-70
9	1660-1960	-100
10	1960-2260	-130
11	2260-2560	-150
12	2560-2860	-170

In G&M3D 1.0, we apply the **Irregular** tool in the Modelling Module to create a density model of the salt dome. This salt dome structure can be approximated by 12 separate irregular bodies located at different depths, each with a constant density, as shown in Table 2. We build these bodies successively using the Modelling Module in G&M3D 1.0. First, we set the range for the source region in the x, y, and z axes to [0 70], [0 70], and [0 50], respectively, using the unit of measurement as hundred meters (hm). The division step is set to be 1×1×1 hm^3. Next, in the Layer-Building interface, we specify the layer number as 28 and the density contrast as -170 kg/m^3. Using **Custom** mode, we outline the geometry of the salt dome at this depth in the workspace, and then we use **Single Click** mode to make slight modifications to its shape. After making these modifications, we save this anomalous body and change the layer number to 27. The copy and paste functions allow us to

https://doi.org/10.5194/egusphere-2025-5357
Preprint. Discussion started: 23 January 2026

visualize the source geometry from the previous layer on the interface, which facilitates anomaly source localization. Users can easily modify the existing layer structure, significantly improving modelling efficiency. This process can be repeated to quickly build the complete salt dome model (Figure 10).

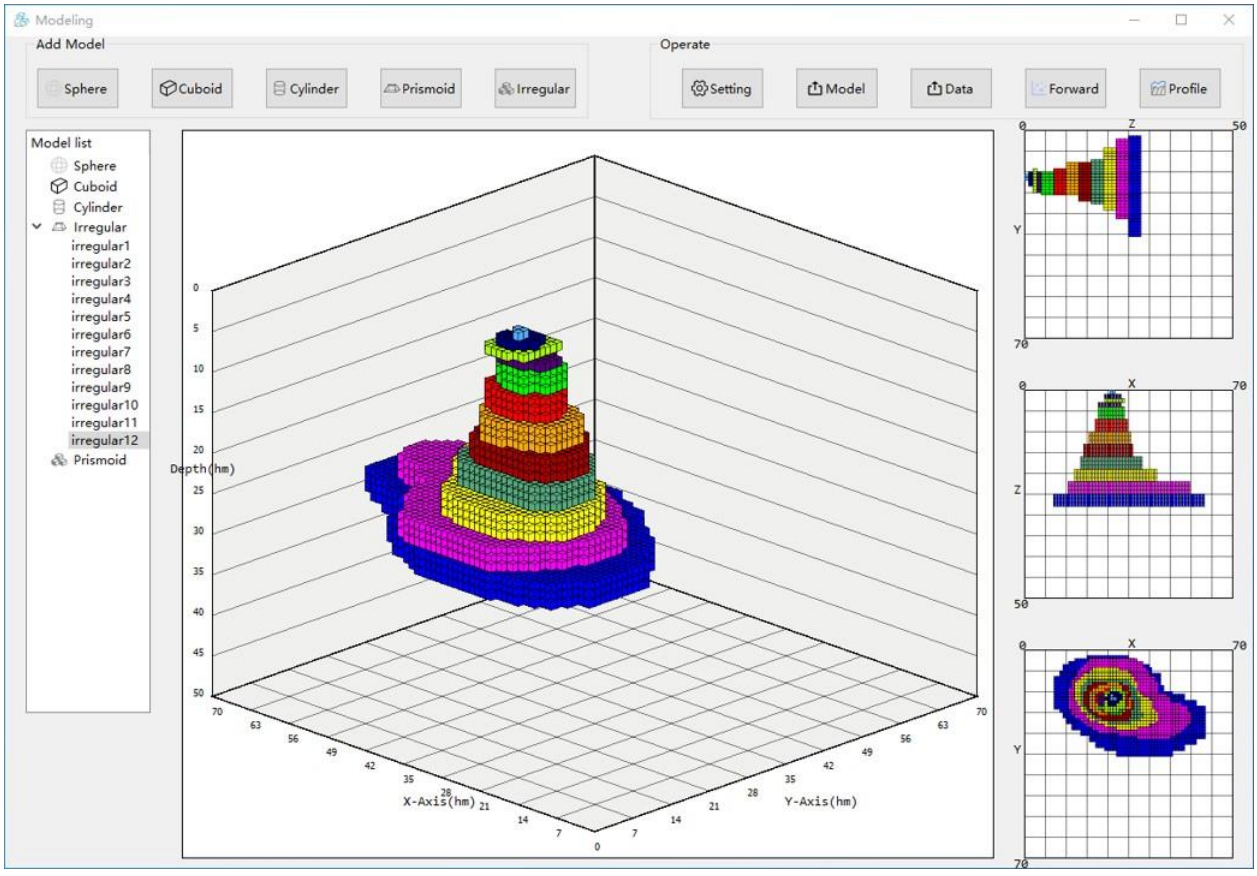

Figure 10: The salt dome model built by G&M3D 1.0.

After constructing the 12 anomalous bodies that form the salt dome model, we use the Forward Modelling Module to calculate the gravity fields and gradients. We set the observation range to match that of the source, with the observation height fixed at 200 m. The resulting gravity fields and gradient components are shown in Figure 11. To validate the accuracy of G&M3D 1.0, a comparative analysis was conducted with spatial domain approaches (Li and Chouteau, 1998). Figure 12 illustrates that the maximum absolute differences remain below 0.03. These data are consistent with the forward simulation results provided by Ennen (2012), confirming the accuracy of the forward calculation in G&M3D 1.0. Additionally, the efficient 3D modelling, forward computation, and visualization processes also highlight the practicality of G&M3D 1.0.

https://doi.org/10.5194/egusphere-2025-5357
Preprint. Discussion started: 23 January 2026

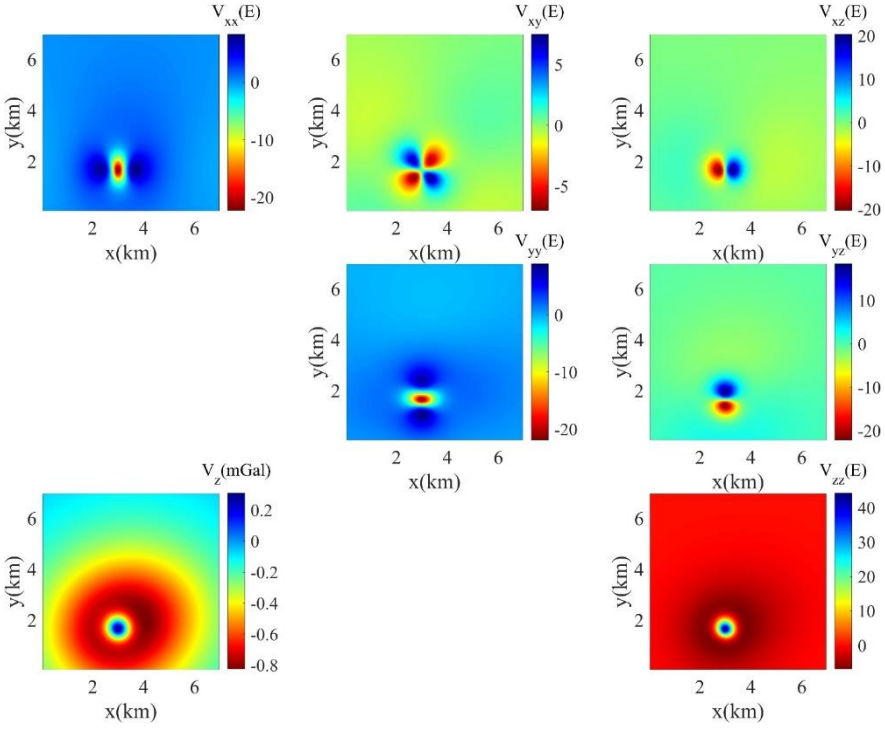

330 **Figure 11: The gravity field and gradient components generated by the salt dome model using G&M3D 1.0.**

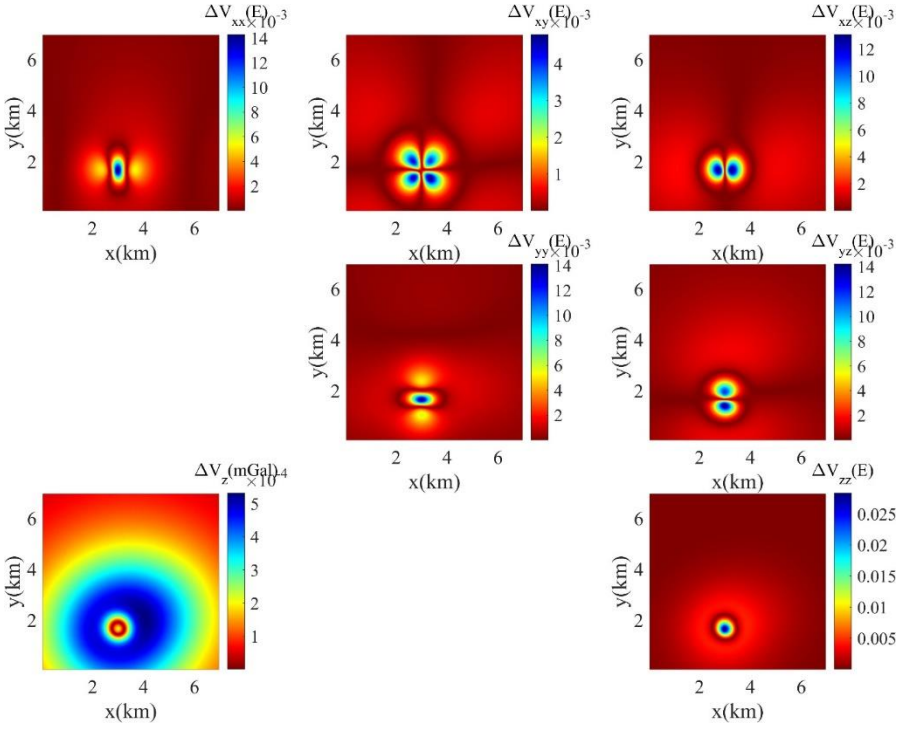

Figure 12: Absolute differences of gravity field and gradient components for salt dome model.

https://doi.org/10.5194/egusphere-2025-5357
Preprint. Discussion started: 23 January 2026

5 Conclusions

The study introduced an open-source software called G&M3D 1.0, developed using the Qt application framework and C++ programming language. G&M3D 1.0 is designed to create 3D models of density and magnetization, as well as to compute their gravity and magnetic fields. Users can run the software both as source code and as a standalone desktop application. With G&M3D 1.0, users can easily create arbitrary source models and perform modifications, deletions, storage, and display of these models. Furthermore, we enhanced the efficient BCE algorithm for forward calculations of gravity gradient tensors and magnetic gradient tensors. Lastly, we demonstrated the gravity modelling over the Vinton salt dome in southern Louisiana, U.S. This practical application illustrates how G&M3D 1.0 can be utilized for geophysical research, training, and data processing and interpretation.

Code and data availability

The G&M3D 1.0 source code used in this study is available at https://doi.org/10.5281/zenodo.17511806 (Wang et al., 2025a). The input and output data presented in this manuscript are available from https://doi.org/10.5281/zenodo.17512457 (Wang et al., 2025b).

Author contribution

Dengkang Wang: Developed the codes, and drafted the paper. Bo Chen: Provided the ideas and their implementation, and revised the paper. Kanggui Wei: Developed the codes, and drafted the paper. Jiaxiang Peng: Provided the initial functions for magnetic forward calculations. Rongwen Guo: Revised the paper.

Acknowledgments

We thank Longwei Chen and Shiyu Zhang for their help in the software development. We thank the High-Performance Computing Center of Central South University for support. The research is supported by the National Natural Science Foundation of China (Grant Nos. 42474123, 42074109).

Declaration of interests

The authors declare that they have no known competing financial interests or personal relationships that could have appeared to influence the work reported in this paper.

https://doi.org/10.5194/egusphere-2025-5357
Preprint. Discussion started: 23 January 2026

References

Bhattacharyya, B., 1964. Magnetic anomalies due to prism-shaped bodies with arbitrary polarization. Geophysics 29, 517-531.

Bhattacharyya, B., Navolio, M., 1976. A fast Fourier transform method for rapid computation of gravity and magnetic anomalies due to arbitrary bodies. Geophys. Prospect. 24, 633-649.

Blakely, R.J., 1996. Potential theory in gravity and magnetic applications. Cambridge University Press.

Caratori Tontini, F., Cocchi, L., Carmisciano, C., 2009. Rapid 3-D forward model of potential fields with application to the Palinuro Seamount magnetic anomaly (southern Tyrrhenian Sea, Italy). J. Geophys. Res. 114.

Chen, L., Liu, L., 2019. Fast and accurate forward modelling of gravity field using prismatic grids. Geophys. J. Int. 216, 1062-1071.

de la Varga, M., Schaaf, A., Wellmann, F., 2019. GemPy 1.0: open-source stochastic geological modeling and inversion. Geoscientific Model Development 12, 1-32.

Ennen, C., 2012. Mapping gas-charged fault blocks around the Vinton Salt Dome, Louisiana using gravity gradiometry data.

Gao, X., 2019. The study and application of 3D inversion methods of gravity & magnetic and their gradient tensor data [Ph. D. thesis]. Changchun: Jilin University.

Guo, Z.H., Guan, Z.N., Xiong, S.Q., 2004. Cuboid Delta T and its gradient forward theoretical expressions without analytic odd points. Chinese Journal of Geophysics-Chinese Edition 47, 1131-1138.

Hassanzadeh, A., Vázquez-Suñé, E., Corbella, M., Criollo, R., 2022. An automatic geological 3D cross-section generator: Geopropy, an open-source library. Environmental Modelling & Software 149, 105309.

Hinze, W.J., von Frese, R.R.B., Saad, A.H., 2013. Gravity and magnetic exploration: Principles, practices, and applications. Cambridge University Press.

Hogue, J.D., Renaut, R.A., Vatankhah, S., 2020. A tutorial and open source software for the efficient evaluation of gravity and magnetic kernels. Computers & Geosciences 144, 104575.

Jessell, M., Aillères, L., De Kemp, E., Lindsay, M., Wellmann, F., Hillier, M., Laurent, G., Carmichael, T., Martin, R., 2014. Next generation three-dimensional geologic modeling and inversion.

Jessell, M., Ogarko, V., De Rose, Y., Lindsay, M., Joshi, R., Piechocka, A., Grose, L., De La Varga, M., Ailleres, L., Pirot, G., 2021. Automated geological map deconstruction for 3D model construction using map2loop 1.0 and map2model 1.0. Geoscientific Model Development 14, 5063-5092.

Li, X., Chouteau, M., 1998. Three-dimensional gravity modeling in all space. Surv. Geophys. 19, 339-368.

Luo, Y., Yao, C., 2007. Forward modeling of gravity, gravity gradients, and magnetic anomalies due to complex bodies. Journal of China University of Geosciences 18, 280-286.

Nagy, D., 1966. The gravitational attraction of a right rectangular prism. Geophysics 31, 362-371.

Nagy, D., Papp, G., Benedek, J., 2000. The gravitational potential and its derivatives for the prism. J. Geod. 74, 552-560.

https://doi.org/10.5194/egusphere-2025-5357
Preprint. Discussion started: 23 January 2026

Okabe, M., 1979. Analytical expressions for gravity anomalies due to homogeneous polyhedral bodies and translations into magnetic anomalies. Geophysics 44, 730-741.

Pirot, G., Joshi, R., Giraud, J., Lindsay, M.D., Jessell, M.W., 2022. loopUI-0.1: indicators to support needs and practices in 3D geological modelling uncertainty quantification. Geoscientific Model Development 15, 4689-4708.

Plouff, D., 1976. Gravity and magnetic fields of polygonal prisms and application to magnetic terrain corrections. Geophysics 41, 727-741.

Qiang, J., Zhang, W., Lu, K., Chen, L., Zhu, Y., Hu, S., Mao, X., 2019. A fast forward algorithm for three-dimensional magnetic anomaly on undulating terrain. J. Appl. Geophys. 166, 33-41.

Thomas, M., 1997. Gravity Prospecting For Massive Sulphide Deposits in the Bathurst Mining Camp, New Brunswick, Canada, pp. 837-840.

Vogel, C.R., 2002. Computational methods for inverse problems. SIAM.

Wang, D., Chen, B., Wei, K., Peng, J., Guo, R. 2025a. GM3D-1.0, Zenodo, https://doi.org/10.5281/zenodo.17511807.

Wang, D., Chen, B., Wei, K., Peng, J., Guo, R. 2025b. G&M3D 1.0: an Interactive Framework for 3D Model Construction and Forward Calculation of Potential Fields [Data set], Zenodo, https://doi.org/10.5281/zenodo.17512458.

Wellmann, J.F., Thiele, S.T., Lindsay, M.D., Jessell, M.W., 2016. pynoddy 1.0: an experimental platform for automated 3-D kinematic and potential field modelling. Geoscientific Model Development 9, 1019-1035.

Wu, L.Y., Tian, G., 2014. High-precision Fourier forward modeling of potential fields. Geophysics 79, G59-G68.

Yuan, Y., Cui, Y., Chen, B., Zhao, G., Liu, J., Guo, R., 2022. Fast and high accuracy 3D magnetic anomaly forward modeling based on BTTB matrix. Chinese Journal of Geophysics-Chinese Edition 65, 1107-1124.

Zhang, Y., Wong, Y.S., 2015. BTTB-based numerical schemes for three-dimensional gravity field inversion. Geophys. J. Int. 203, 243-256.

Zhao, G., Chen, B., Chen, L., Liu, J., Ren, Z., 2018. High-accuracy 3D Fourier forward modeling of gravity field based on the Gauss-FFT technique. J. Appl. Geophys. 150, 294-303.